5-1-2016

The role of bone sialoprotein in the tendon-bone insertion

Ryan Marinovich
Western University

Yohannes Soenjaya
Western University

Gregory Q. Wallace
Western University

Andre Zuskov
University of Pennsylvania Perelman School of Medicine

Andrew Dunkman
University of Pennsylvania Perelman School of Medicine

See next page for additional authors

HHS Public Access

Author manuscript

Matrix Biol. Author manuscript; available in PMC 2017 May 01.

Published in final edited form as:

Matrix Biol. 2016 ; 52-54: 325–338. doi:10.1016/j.matbio.2016.01.016.

The Role of Bone Sialoprotein in the Tendon-Bone Insertion

Ryan Marinovich[1,*], **Yohannes Soenjaya**[2,*], **Gregory Q. Wallace**[3], **Andre Zuskov**[4], **Andrew Dunkman**[4], **Brian L. Foster**[5,**], **Min Ao**[6], **Kevin Bartman**[1], **Vida Lam**[7], **Amin Rizkalla**[2,7], **Frank Beier**[8], **Martha J. Somerman**[6], **David W. Holdsworth**[9], **Louis J. Soslowsky**[4], **François Lagugné-Labarthet**[3], and **Harvey A. Goldberg**[1,7]

[1]Department of Biochemistry, University of Western Ontario, London, ON, Canada

[2]Biomedical Engineering Program, University of Western Ontario, London, ON, Canada

[3]Department of Chemistry, University of Western Ontario, London, ON, Canada

[4]McKay Orthopaedic Research Laboratory, University of Pennsylvania, Philadelphia, PA

[5]Division of Biosciences, College of Dentistry, The Ohio State University, Columbus, OH, USA

[6]National Institute of Arthritis and Musculoskeletal and Skin Diseases (NIAMS), National Institutes of Health (NIH), Bethesda, MD, USA

[7]School of Dentistry, University of Western Ontario, London, ON, Canada

[8]Department of Physiology and Pharmacology, University of Western Ontario, London, ON, Canada

[9]Departments of Surgery and Medical Biophysics, University of Western Ontario, London, ON, Canada

Abstract

Tendons/ligaments insert into bone via a transitional structure, the enthesis, which is susceptible to injury and difficult to repair. Fibrocartilaginous entheses contain fibrocartilage in their transitional zone, part of which is mineralized. Mineral-associated proteins within this zone have not been adequately characterized. Members of the Small Integrin Binding Ligand N-Linked Glycoprotein (SIBLING) family are acidic phosphoproteins expressed in mineralized tissues. Here we show that two SIBLING proteins, bone sialoprotein (BSP) and osteopontin (OPN), are present in the mouse

Corresponding author: Harvey A. Goldberg, School of Dentistry, Schulich School of Medicine and Dentistry, University of Western Ontario, London, Ontario, Canada N6A 5C1, ; Email: hagoldbe@uwo.ca, Telephone: 519-661-2182.

*Authors contributing equally to this work

**Research was completed while a Fellow at NIAMS/NIH

AUTHOR CONTRIBUTIONS

R. Marinovich and Y. Soenjaya, contributed to conception, design, data acquisition, analysis, and interpretation, drafted and critically revised the manuscript; G. Wallace, A. Zuskov, A. Dunkman, M. Ao, V. Lam and K. Bartman contributed to data acquisition and interpretation; B. Foster and M. Somerman contributed to conception, evaluation and interpretation; L. Soslowsky, F. Lagugné-Labarthet, D. Holdsworth, F. Beier and A. Rizkalla contributed to design, data analysis and interpretation; H. Goldberg, contributed to conception, design and interpretation, drafted and critically revised the manuscript. All authors critically revised the manuscript.

The authors declare no potential conflicts of interest with respect to the authorship and/or publication of this article.

enthesis. Histological analyses indicate that the calcified zone of the quadriceps tendon enthesis is longer in *Bsp*$^{-/-}$ mice, however no difference is apparent in the supraspinatus tendon enthesis. In an analysis of mineral content within the calcified zone, micro-CT and Raman spectroscopy reveal that the mineral content in the calcified fibrocartilage of the quadriceps tendon enthesis are similar between wild type and *Bsp*$^{-/-}$ mice. Mechanical testing of the patellar tendon shows that while the tendons fail under similar loads, the *Bsp*$^{-/-}$ patellar tendon is 7.5% larger in cross sectional area than wild type tendons, resulting in a 16.5% reduction in failure stress. However, picrosirius red staining shows no difference in collagen organization. Data collected here indicate that BSP is present in the calcified fibrocartilage of murine entheses and suggest that BSP plays a regulatory role in this structure, influencing the growth of the calcified fibrocartilage in addition to the weakening of the tendon mechanical properties. Based on the phenotype of the *Bsp*$^{-/-}$ mouse enthesis, and the known *in vitro* functional properties of the protein, BSP may be a useful therapeutic molecule in the reattachment of tendons and ligaments to bone.

Keywords

bone sialoprotein; osteopontin; enthesis; quadriceps tendon; supraspinatus tendon; calcified fibrocartilage

1. INTRODUCTION

Members of the Small Integrin Binding Ligand N-linked Glycoprotein (SIBLING) protein family are associated with the mineralized tissues of the skeleton and dentition [1]. SIBLINGs are anionic phosphoproteins with a flexible structure and extensive post-translational modifications. The family consists of 5 members: bone sialoprotein (BSP), osteopontin (OPN), dentin matrix protein 1 (DMP1), dentin sialophosphoprotein (DSPP) and matrix extracellular phosphoglycoprotein (MEPE), with the encoding genes located in a syntenic gene locus on murine chromosome five [1].

BSP is a heavily glycosylated and phosphorylated protein that is expressed at the onset of mineralization in hard connective tissues [2]. In cell-free systems, BSP has been demonstrated to be a potent nucleator of hydroxyapatite (HA), the principal mineral component of bone [3]. Nucleation and binding to HA by BSP is conferred by polyglutamic acid sequences found in the central region of the protein [3,4]. BSP also contains an N-terminal collagen-binding domain and it is proposed that binding of BSP to collagen promotes HA nucleation [5,6]. Finally, BSP contains an integrin-binding RGD motif, located towards the C-terminus, which promotes osteoblast differentiation and matrix mineralization [7].

Mice in which the *Bsp* gene has been ablated (*Bsp*$^{-/-}$) have a variety of skeletal and dental defects [8]. At 4 months of age, these mice display reduced long-bone length and cortical thickness, and a lower rate of bone formation, but have higher trabecular bone density than wild type mice [9]. However, due to incisor malocclusion phenotype on hard diet, some of these defects are ameliorated if *Bsp*$^{-/-}$ mice are fed a soft food diet [10]. Further studies by the Malaval group showed that the *Bsp*$^{-/-}$ mouse displays a delay of bone repair in cortical

injury models [11] and impaired bone formation and resorption in marrow ablation models [12].

More recently, a significant periodontal phenotype has been uncovered in the *Bsp*$^{-/-}$mouse. Acellular cementum is a thin mineralized tissue found along the cervical portion of the root of the tooth, into which the periodontal ligament (PDL) inserts. Immunohistochemistry shows that acellular cementum is rich in BSP, and in the *Bsp*$^{-/-}$ mouse there is a striking reduction in cementum deposition [13]. Additionally, the *Bsp*$^{-/-}$ mouse PDL is disorganized, with poorly aligned collagen fibers that do not properly insert into the tooth root [10,13,14]. However, insertion of the PDL collagen into alveolar bone appears normal [14].

The defects observed in the PDL of the *Bsp*$^{-/-}$ mouse have spurred us to investigate other junctions between soft and mineralized tissue. Of particular interest is the enthesis, the transition site of tendon and ligament insertion into bone. Fibrocartilaginous entheses are found where tendons or ligaments attach to the epiphysis or apophysis of long bones [15]. As such, they are present at several key sites involved in locomotion, such as where the supraspinatus tendon (SST) of the rotator cuff meets the epiphysis of the humerus, and where the quadriceps tendon (QCT) inserts into the back of the patella.

Fibrocartilaginous entheses contain a fibrocartilage zone containing type II, IX, X collagen and fibrochondrocytes at the interface between tendon and bone [16]. Fibrocartilaginous entheses display 4 transitional zones: the dense connective tissue of the tendon, uncalcified fibrocartilage (UFC), calcified fibrocartilage (CFC), and bone. A sharp boundary occurs between the calcified and uncalcified fibrocartilage which is known as the tidemark. Entheses are largely avascular and as such, have a limited potential for regeneration [15,17]. Once torn away from bone, reattachment of a tendon or ligament is difficult. Indeed, the failure rates for repairs of massive rotator cuff tears remain high despite advances in surgical technique [18].

Given its HA nucleating and collagen binding properties, and the phenotype observed in the *Bsp*$^{-/-}$ mouse PDL, we hypothesize that BSP is present in fibrocartilaginous entheses and is involved in directing the mineralization and organization of these structures. In this study we show for the first time that the mineralized zones of murine fibrocartilaginous entheses contain the SIBLING proteins BSP and OPN, and that the loss of BSP results in a morphological abnormality of the QCT enthesis as well as a mechanical defect in the patellar tendon.

2. RESULTS

2.1 BSP and OPN are present in the mineralized tissues of fibrocartilaginous entheses

Immunohistochemistry was performed to identify BSP in the murine fibrocartilaginous entheses. BSP was detected in the calcified fibrocartilage (CFC) of the QCT and SST entheses, as well as the adjacent bone (Fig. 1). Additionally the presence of OPN was identified in the enthesis, and its tissue distribution mimics that of BSP. The absence of BSP

and OPN immunostaining in the mineralized tissues was confirmed in *Bsp*$^{-/-}$ and *Opn*$^{-/-}$ mice, respectively (Fig. 1).

2.2 Bsp$^{-/-}$ mice exhibit abnormalities in the calcified fibrocartilage of the enthesis

In order to study BSP's role in the murine fibrocartilaginous enthesis, histological characterization of two selected entheses was performed. The QCT enthesis was chosen due to its large size, as well as ease of access. It was thought that differences between wildtype and *Bsp*$^{-/-}$ animals would be more pronounced in a larger enthesis. The SST enthesis was chosen due to its medical relevance, as avulsion of the SST from the humeral head is a common rotator cuff injury.

Tide mark to bone lengths (corresponding to the CFC) in 15 week-old *Bsp*$^{-/-}$ entheses were measured (Fig. 2A,B,E,F, Table 1, Supplemental Fig. 1). At 15 weeks of age, there is a 28% increase over wild type in the length of the QCT CFC in *Bsp*$^{-/-}$ mice ($p<0.05$, n=5). In addition, 14 month-old wild type and *Bsp*$^{-/-}$ entheses were analyzed (Table 1). Although the availability of mice at this time point was limited (n=3), older *Bsp*$^{-/-}$ animals did trend towards an increase with an extension in length of 41% over littermate wild type animals of the same age (Table 1). No difference was observed in wild type QCT CFC lengths between the 15 week and 14 month age groups. In contrast, SST CFC lengths did not significantly differ between wild type and *Bsp*$^{-/-}$ mice in either age group (Fig. 2E–H). Von Kossa staining of the QCT and SST enthesis indicate approximately equivalent mineral content in the CFC of the wild type and *Bsp*$^{-/-}$ 15 week old mouse enthesis (Fig. 2C,D,G,H).

As BSP is postulated to play a direct role in mineral deposition, mineralization analysis was initially performed using micro-CT. The QCT enthesis was again chosen for this analysis in part because of the previously highlighted abnormality in the length of this enthesis in *Bsp*$^{-/-}$ mice and also due to the ease of locating this structure using microCT. Discerning the exact location of enthesis CFC via microCT is normally difficult since CFC and bone have similar radioopacity, however the location of the QCT CFC is relatively easy to determine as it occupies the majority of the posterior of the patella. Furthermore, by delineating a 3-D volumes of interest (VOI), we were able to minimize the contribution of bone to the mineral density measurements.

We analyzed the degree of mineralization along the length of the QCT enthesis. Micro-CT analysis demonstrated that radiodensity in the region corresponding to the CFC of the QCT enthesis increased rapidly and then plateaued (Fig. 3A,B). No statistically significant difference in radiodensity was observed between wild type and *Bsp*$^{-/-}$ mice, suggesting that mineral content in the *Bsp*$^{-/-}$ QCT enthesis is normal (Fig. 3C,D). A slight increase in radiodensity was observed in the region immediately after the tidemark (region of interest: 0.04–0.08 mm) of the *Bsp*$^{-/-}$ QCT enthesis compared to wild type, suggesting that higher levels of mineral are present in this region in the *Bsp*$^{-/-}$ mouse, however the difference was not statistically significant (Fig. 3A,B).

Previously, the mineral gradient that occurs at the tidemark was measured to be approximately 20 μm in length, and this length was constant at several developmental timepoints [20]. Of relevance, past studies have shown that a gradient of mineral is present

along the enthesis where it is believed to play a role in stress dissipation [19,20]. Since the resolution of the micro-CT analysis was limited to 13.5 μm, to obtain more definitive analysis, Raman spectroscopy, which has a resolution of approximately 0.5–0.75 μm, was used to determine the gradient of mineral content. An additional advantage of Raman spectrocopy is that scan points were initally determined using light microscopy, making the distinctions between the zones of the enthesis obvious. Thus, the exact location of the tidemark as well as the CFC-bone junction are well defined, ensuring that only CFC was measured.

We used Raman spectrocopy to analyse the relative difference in intensity between the P-O bonds (peak at 960 cm^{-1}) of phosphate ions of HA to the organic C-H bonds (peak at 2940 cm^{-1}) of the organic matter present in the tissue (mostly collagen), in *Bsp*$^{-/-}$ and wild type mice (Fig. 4A). Raman analysis mirrored our micro-CT findings. Mineral content increases rapidly at the tidemark in both *Bsp*$^{-/-}$ and wild type mice and then plateaued, with relatively equal levels of mineral being present in both sets of mice (Fig. 4B). Similar to micro-CT analysis, there appears to be a minor increase in mineral near the tidemark (first 10–15 μm past the tidemark), based on the analyses of individual *Bsp*$^{-/-}$ mice (Fig. 4C,D); however, due to the highly variable nature of Raman signals, statistical significance was not found ($p>0.05$).

2.3 Mechanical testing suggests a weakened patellar enthesis in Bsp$^{-/-}$ mice

Abnormalities noted in the CFC of the QCT enthesis prompted us to determine whether the strength of *Bsp*$^{-/-}$ enthesis is compromised. Ideally the strength of the QCT would be determined directly; however, mechanical studies on this particular tendon are not as easily done as the patellar tendon. The QCT is a short tendon which connects the muscles of the quadriceps to the posterior of the patella. As such the proximal end of the QCT cannot be mounted into the mechanical testing apparatus. Instead the strength of the patellar tendon, which connects the anterior of the patella to the proximal tibia, was analyzed.

Mechanical testing performed on the patellar tendon, which links the patella to the proximal end of the tibia, indicated that its cross-sectional area was approximately 7.5% larger in *Bsp*$^{-/-}$ mice than wild type ($p<0.05$)(Fig. 5A). The load required to fail the patellar tendon is similar for both genotypes (Fig. 5D). Although the failure loads are the same, the failure stress, which is load per cross-sectional area, is decreased by 16.5% ($p<0.05$), indicating that *Bsp*$^{-/-}$ mice have a weaker patellar tendon compared to wild type ($p<0.05$) (Fig. 5B). Regardless of genotype, the patellar tendon failed at different positions along its length, with some failures occurring at the enthesis while others occurred at the tendon midsubstance and, in some cases, failed at more than one location (Fig. 5C). Unexpectedly, the local elastic moduli of *Bsp*$^{-/-}$ patellar tendon at three different regions: 1) patellar insertion, 2) midsubstance, and 3) tibial insertion, were found to be similar to wild type (Fig. 5G–I). In addition, the overall percent relaxation and stiffness of the *Bsp*$^{-/-}$ patellar tendon were not affected (Fig. 5E,F).

2.4 Collagen organization is not affected by the loss of BSP

Given the mechanical deficit observed, as well as the disorganization seen in the periodontal ligament [13], collagen organization was assessed by picrosirus red staining. Images of wild type and *Bsp*$^{-/-}$ SST and QCT entheses were taken using circularly polarized light (Fig. 6). No striking difference in collagen organization was observed.

3. DISCUSSION

BSP is an extracellular matrix protein present in mineralized tissues including bones and teeth. Here we demonstrate for the first time that BSP is also present in the CFC zone of the fibrocartilaginous enthesis. OPN was identified for the first time in this structure as well. The absence of BSP resulted in a lengthening of the CFC in the QCT enthesis. Furthermore, the *Bsp*$^{-/-}$ patellar tendon has an increased cross-sectional area and lower failure stress, however, the overall collagen organization and mineral content of the *Bsp*$^{-/-}$ QCT enthesis appeared to be normal. Our findings suggest that BSP plays a role, though undefined, in the fibrocartilaginous enthesis.

3.1 Role of altered calcified fibrocartilage zone of the Bsp$^{-/-}$ QCT enthesis

In this study, we have shown that BSP, a protein with demonstrated potency to promote mineral formation *in vitro* [3], is present in the CFC zone of the enthesis. In the same tissue, we also demonstrated the presence of OPN, a close relative of BSP with inhibitory activity on HA formation [21]. The extracellular matrix composition of fibrocartilaginous entheses has been investigated previously [16,22,23], however these studies primarily focused on the various collagens and proteoglycans. The distribution of mineral and orientation of the collagen fibers in the enthesis has been shown to influence its mechanical properties [19,24,25,26,27]. Recent studies have indicated that the Indian Hedgehog signaling pathway is involved in enthesis development and mineralization of the CFC, in part because its ablation results in decreased mineralization and less collagen imbedded in the mineralized tissues [28,29,30,31]. Similarly, alkaline phosphatase, whose expression is correlated to mineral formation, is expressed by the differentiated fibrocartilaginous cells [29]. To our knowledge, the presence of the SIBLING family of mineral-associated and mineral-modulating proteins has never been reported in the enthesis.

Our previous studies have shown that acellular cementum is deficient in the *Bsp*$^{-/-}$ mice, which resulted in periodontal ligament (PDL) detachment and disorganization, and associated periodontal tissue breakdown such as resorption of alveolar bone and tooth surface [13]. Minimizing the mechanical load during mastication, by changing to a soft diet, was not successful in ameliorating the rate of periodontal breakdown [10]. In spite of this, reducing the mechanical load significantly reduced the rate of incisor malocclusion, which affected the ability of *Bsp*$^{-/-}$ mice to feed normally. Based on the disorganization and detachment in the PDL, we initially hypothesized that the loss of BSP would have a negative effect on the collagen structure of the enthesis. However, the absence of changes in collagen organization in the CFC of *Bsp*$^{-/-}$ mouse enthesis suggests that BSP does not play a role in this.

In the absence of BSP, the calcified fibrocartilage of the enthesis still forms and becomes mineralized. Furthermore, based on microCT and Raman spectroscopy the mineral density of the *Bsp*$^{-/-}$ QCT enthesis at 15 weeks appears relatively normal. Thus it is of interest that at 15 weeks, the *Bsp*$^{-/-}$ QCT enthesis is greater in length (28% increase) compared to wild type mice and that at 14 months the QCT CFC length appears to increase in the *Bsp*$^{-/-}$ mice but not wild type mice. These results indicate that CFC growth is dysregulated in BSP's absence. While unexpected we can only speculate the reasons for this at the present time. The CFC helps to anchor the tendons or ligaments to the bone and withstand tensile and shear loads under minimal movement. The enthesis fibrocartilage is a dynamic tissue that responds to mechanical load. Thus, the observed increased length in the QCT of the CFC zone is likely a compensation to strengthen the CFC-bone interface by allowing for greater dissipation of stress.

Extensions of the mineralized zones of entheses have been documented in other studies. Polisson *et al.* have reported lengthening of the mineralized tissues of tendon and ligament insertions in humans suffering from X-linked hypophosphatemic osteomalacia [32]. Utilizing a murine model of this disorder in which *PHEX*, a gene involved in phosphate regulation, has been inactivated, Liang *et al.* have shown lengthening of the CFC in the QCT enthesis as well as in the Achilles tendon insertion into the calcaneus and the attachment of the patellar tendon to the tibial tubercle [33]. Interestingly, a related disorder, autosomal recessive hypophosphatemia, is caused by a loss of function mutation in DMP1 [34], which is also part of the SIBLING protein family [1]. Characterization of the *Dmp1*$^{-/-}$ fibrocartilaginous enthesis, however, has not yet been described.

A curious observation of these studies is that while alterations are present in the mineralized tissues of the QCT enthesis, there are no apparent histological changes in the SST enthesis. The observation may be due to the different mechanical forces experienced by the SST and QCT entheses. For example, in entheses that display a large change in insertional angle during joint movement, a larger region of uncalcified fibrocartilage (UFC) is observed [15,35]. Because this enthesis zone is more pliable than either tendon or the CFC, researchers have hypothesized that the increased size of the UFC aids in smooth movement of the joint during its total range of movement. Gao and Messer suggest that the size of the CFC is determined by the tensile load that the enthesis experiences at puberty [36]. When the shoulder muscles of newborn mice were paralyzed with botulinum toxin, decreased mineralization near the SST enthesis in the bone was observed at 21 days of age and fibrocartilage failed to form at the insertion [37].

The quadriceps muscles are some of the largest and most powerful muscles in the body, in both mice and humans. Located on the anterior surface of the femur, they are involved in the extension of the leg and are used extensively during locomotion. The QCT inserts directly into the back of the patella. As such, the tensile force on the QCT enthesis under load is large and the insertional angle is small. In contrast, the supraspinatus muscle is located in the shoulder and its contraction drives abduction at the shoulder joint and exterior rotation of the arm. The muscle is smaller than the quadriceps muscles and produces loads of a lower magnitude. Furthermore the SST makes contact with bone at an oblique angle, wrapping around the head of the humerus before inserting at the SST enthesis. As such, the nature of

the loads in the QCT and SST entheses are quite different, and these differences may be the cause of the discrepancies in phenotypes observed in the *Bsp*$^{-/-}$ mouse.

3.2 Bsp$^{-/-}$ patellar tendon exhibits weakened mechanical properties under load

Interestingly, the *Bsp*$^{-/-}$ patellar tendon cross-sectional area is greater than the wild type; however, under mechanical testing, the *Bsp*$^{-/-}$ patellar tendon failed at a similar applied load compared to wild type. This implies that the *Bsp*$^{-/-}$ patellar tendon is weaker, as a tendon of larger cross-sectional area is expected to fail at higher loads. It is possible that a larger patellar tendon cross-sectional area observed in the *Bsp*$^{-/-}$ mouse is a compensatory mechanism that ensures that although the tendon is weaker, it can withstand the same loads. Mentioned previously, Gao and Messer have hypothesized that the size of the CFC in an enthesis is related to the tensile load under which it is placed during its use [36]. The increased size of the QCT CFC in the *Bsp*$^{-/-}$ mouse may also be compensating for a weakened tendon. Challenge experiments in which greater stress is placed on the *Bsp*$^{-/-}$ enthesis may provide insight as to how mechanical factors impact BSP's role in enthesis mineralization.

Challenge experiments may also reveal a more profound defect caused by the loss of BSP due to compromised repair processes in the enthesis. BSP has been implicated in the repair of several mineralized tissues. When BSP and collagen (prepared by crosslinking BSP to collagen, personal communication E. Salih) are implanted into calvarial defects of 7–8 week old rats, new bone formation is observed [38]. Cortical defects drilled into the femurs of *Bsp* $^{-/-}$ mice heal slowly when compared to wild type counterparts [11,39]. Indeed, given BSP's collagen binding domain, hydroxyapatite nucleating properties and cell attachment, signaling and migration functions, BSP may be an attractive molecule to promote repair in common entheseal injuries such as rotator cuff tears, however further characterization of BSP's role in enthesis development is required.

Interestingly, there are many similarities between the development of fibrocartilaginous entheses and growth plates involved in endochondral ossification [40]. We and others have recently identified abnormalities in the growth plates of *Bsp*$^{-/-}$ mice as well as a delay in mineral deposition during endochondral ossification [41,42]. By 8 weeks however, *Bsp*$^{-/-}$ mice display a normal bone length when fed a soft food diet [10]. This suggests that a more pronounced phenotype may be present during the development of *Bsp*$^{-/-}$ fibrocartilaginous entheses.

These studies have identified the SIBLING proteins BSP and OPN in the CFC of the murine fibrocartilaginous enthesis, showing for the first time the presence of these mineral associated proteins in the enthesis. The enthesis phenotype of mice that lack BSP was examined in order to elucidate the role of BSP in enthesis fibrocartilage. In the absence of BSP, the growth of the CFC appears to be dysregulated in the QCT enthesis, which continues to increase in size well into adulthood. In the absence of BSP, the body may compensate with an increase in the cross-sectional area of tendons in the Bsp$^{-/-}$ mouse as was observe in the platellar tendon. Due to the known properties of BSP, it may still be involved at the mineralization front of the fibrocartilaginous enthesis where it likely contributes to a complex network of proteins, which act to control the growth of the CFC

and regulate mineral deposition in the enthesis. As such, BSP may ultimately prove to be a useful molecule in the reattachment of tendons and ligaments into bone.

4. MATERIALS AND METHODS

4.1 Animals

Animal care followed guidelines of the Canadian Council on Animal Care and Veterinary Services at the University of Western Ontario (Protocol #: 2008-092). Preparation and genotyping of *Bsp*$^{-/-}$ and wild type mice, maintained on a mixed 129/CD1 background, were performed as described previously [9]. *Opn*$^{-/-}$ mice were obtained from Jackson Laboratory (JAX Stock number 004936, Sacramento, USA) and handled as described previously [43]. All mice used in this study were fed a soft diet as previously outlined [10] and were sacrificed as required by CO_2 asphyxiation. All comparisons between genotypes were performed on male mice born in the same litter.

4.2 Histology and Immunohistochemistry

Wild type and *Bsp*$^{-/-}$ shoulder and knee joints from 15 week old mice were harvested and prepared for histology as described previously, with alterations [44]. Briefly, tissues were fixed in neutral buffered formalin (10%) overnight at 4°C and were then decalcified in 0.65 M EDTA pH 7.4 at 37°C for three weeks. Tissues were processed by University Hospital Pathology Core, London, ON, Canada, then embedded in paraffin and sectioned into 5 μm sections.

Immunohistochemical analysis was performed as described previously [13,42]. Sections were treated overnight at 4°C with rabbit anti-mouse BSP serum (courtesy of Dr. Renny Franceschi, University of Michigan School of Dentistry, Ann Arbor, MI), diluted 1:200 times in 5% goat serum in phosphate buffered saline (PBS), or rabbit anti-mouse OPN serum (LF-175, courtesy of Dr. Larry Fisher, NIDCR, NIH, Bethesda, MD) diluted 1:200 times in 5% goat serum in phosphate buffered saline (PBS).

Hematoxylin and eosin staining was performed with Harris's Hematoxylin (Sigma-Aldrich) and Eosin Y (Sigma-Aldrich). Whole tissue von Kossa staining was performed as previously described [45] (Tripp and Mackay, 1972). Briefly, undecalcified tissues were fixed and immersed in a 2% silver nitrate solution for 2 days. Silver ions were then reduced and precipitated within the samples using 0.6 M sodium hypophosphite then decalcified in 10% formic acid and embedded in paraffin for sectioning.

For picrosirius red staining tissues were stained with Sirius red (Sigma-Aldrich) in saturated picric acid for 1 hour. Following staining, sections were washed in two changes of acidified water, then dehydrated and cleared. Specimens were imaged using circularly polarized light.

All solutions used in these protocols were made with Milli-Q deionized water unless otherwise indicated.

4.3 Measurement of the calcified fibrocartilage zone

In H&E stained images, the distance between the tidemark and bone of the SST and QCT entheses were measured across three transverses drawn parallel to the known orientation of the collagen fibers based on picrosirius red staining. Measurements were performed by two blinded individuals, in five 15 week-old and three 14 month-old male wild type and *Bsp*$^{-/-}$ litter mate pairs. Bone-CFC junction was identified by the sharp but irregular boundaries between the CFC and the osteons of bone (Shown in Figure S1). The lengths of the triplicate measurements in each enthesis were averaged and these averages were compared between wild type and *Bsp*$^{-/-}$ mice using a parametric unpaired t-test.

While all measurements were made in the sagittal plane on the QCT enthesis, particular attention was made to minimize potential differences due to the angle of the plane of sectioning. Given the number of individual samples measured and the size of the difference observed between wild type and *Bsp*$^{-/-}$ CFC lengths, it is unlikely that the minor variations of the plane of the sectioning introduced major artifactual discrepancies.

4.4 Mechanical testing

Immediately after euthanization, the hind limbs (n =15 per genotype) of 15 week old mice were removed and wrapped in phosphate buffered saline (PBS) soaked gauze, then stored at −20°C prior to mechanical testing. After thawing, the skin of the contralateral limbs was removed and the patella-patellar tendon-tibia complexes were carefully dissected under magnification, as described previously [46]. The tendon cross-sectional area was measured using a custom laser-based device. The anterior surface of each tendon was speckle-coated with Verhoeff's stain to facilitate optical strain measurement. Prior to mechanical testing, the tibia was potted in polymethyl methacrylate (PMMA) and the patella was gripped with custom aluminum fixtures. The specimens were then loaded into a materials testing system (Instron, Model 5848; Norwood, MA, USA) with a 10 N load cell. Throughout the testing, the specimen and fixtures were submerged in a PBS bath maintained at 37°C. All specimens were tested using a modified version of the protocol outlined in Dunkman *et al.* [46]. Briefly, the protocol consisted of preloading and preconditioning followed by 300 second hold and stress relaxation at 5% strain. After a return to gauge length, a ramp to failure at 0.1%/s was performed to measure the failure load of the specimens. For data analysis, modulus was calculated using optical tracking software for each tendon at three regions: (1) the patellar origin (1 mm distal to the patella), (2) tendon mid-substance and (3) tibial insertion (1 mm proximal to tibial insertion).

4.5 Microcomputed Tomography

Microcomputed tomography (μCT) analysis of the patella was performed prior to decalcification using the eXplore Locus SP scanner (GE Healthcare, London, ON, Canada). 2D images were acquired using an X-ray tube with a voltage of 80 kVP and a current of 80 μA, with a 0.508 mm Al filter. The exposure interval time of the scanner was 1600 msec/frame at 4 frames/view. In total, 900 views were obtained at 0.4 degrees angular increments. The data were reconstructed at a spatial resolution of 13.5 μm. All reconstructed data were calibrated with a cortical bone phantom (SB3; Gammex RMI, Milwaukee, WI, USA) with a

hydroxyapatite equivalent of 1,100 mg/cc (White 1978), as well as water and air. Data were analyzed with MicroView ABA version 2.2 (GE Healthcare).

For patellar analysis, 5 mice per genotype were used. Quantification of mineral density was performed on 3D cubical volumes of interest (VOIs; 20 × 20 × 20 voxels) identified at the base area, where attachment of the quadriceps tendon occurred.

For measurement of mineral density distribution along the tendon-to-bone insertion, three parallel transverse line measurements were obtained and averaged for each region of interest (ROI). The lines were defined manually along the CFC of the QCT enthesis.

4.6 Raman spectroscopy

Three pairs of male wild type and *Bsp*$^{-/-}$ littermates aged 15 weeks were euthanized, and the patellae were carefully dissected out immediately following death. Patellae were then immersed in optimal cutting temperature (O.C.T) media (Tissuetek) and snap frozen. Sagittal sections (10 μm) of the patellae were cut in a cryostat, sections were quickly fixed, washed and dehydrated using an ethanol gradient, and then stored −80°C until scanning.

The apparatus used for Raman spectroscopy was a LabRAM HR (Horiba-Jobin-Yvon, Kyoto Japan) combined with an inverted optical microscope (IX71, Olympus, Tokyo, Japan) and interfaced with a piezoelectric positioning stage (TAO stage, JPK Instruments Inc., Berlin, Germany). The protocols used were adapted from those described by Schwartz *et al.* [20]. Raman spectra were collected using an excitation source of 632.8 nm with a power of 10 mW at the sample. The beam was focused onto the sample surface by a 100× objective (N.A. 0.9) allowing for a beam diameter between 0.5 and 0.75 μm. A grating of 600 grooves/mm was used and the pinhole of the spectrometer was opened to 200 μm. Each spectra was collected between 200 and 4000 cm^{-1} for 10 seconds and averaged over 5 accumulations. The sample was preliminary step-scanned with 1 μm step between successive points. Scans were performed along a line crossing the tide mark, the Raman spectra of which was used to confirm precise location of the mineral interface. Once the tide mark was identified, Raman spectra were then collected using 20 μm intervals.

Peak intensity (height) was measured at 960 cm^{-1}, representing the P-O bonds of hydroxyapatite, and 2940 cm^{-1}, representing the C-H bonds of collagen and other proteins. After baseline correction, the P-O peak was normalized to the C-H peak, based on the assumption that the collagen content of the sample was constant at all points measured. Normalized 960 cm^{-1} hydroxyapatite P-O peak intensities were then compared between wild type and *Bsp*$^{-/-}$ samples. For each individual QCT enthesis, three separate linear measurements were made per enthesis, as described in the figure legends, lines of measurement were drawn from tidemark to bone in the orientation of the collagen fibers of the CFC.

4.7 Statistical analyses

Quantitative data are expressed as mean ± standard deviation. For enthesis length and mechanical comparisons, statistical analyses between experimental groups were performed using an unpaired parametric t-test. For micro-CT and Raman spectroscopy, differences

between wild type and $Bsp^{-/-}$ mice were investigated using repeated measures two way ANOVA. All statistical analysis were performed with Prism version 6.00 (GraphPad Software, La Jolla, CA).

Supplementary Material

Refer to Web version on PubMed Central for supplementary material.

Acknowledgments

This research was supported by the Canadian Institutes for Health Research (CIHR) (FRN130572 - HAG), the Intramural Research Program of the National Institute of Arthritis and Musculoskeletal and Skin Diseases (NIAMS) of the National Institutes of Health (NIH) (MJS), NIAMS grant AR 066110 (BLF), and at the Penn Center for Musculoskeletal Disorders (NIH/NIAMS, P30 AR050950 - LJS). YS was supported by The Joint Motion Program, a CIHR funded Strategic Training Initiative in Health Research (STIHR), and the AO Foundation (Davos, Switzerland). FLL and GQW contribution to this work was supported by the Natural Science and Engineering Research Council Discovery grant program. VL was supported by an Ontario Dental Association sponsored studentship provided through the Schulich Dentistry Summer Student Research Program.

References

1. Fisher L, Fedarko N. Six Genes Expressed in Bones and Teeth Encode the Current Members of the SIBLING Family of Proteins. Connect Tissue Res. 2010; 44:33–40. [PubMed: 12952171]
2. Goldberg, HA.; Hunter, GK. Functional domains of bone sialoprotein. In: Goldberg, M., editor. Phosphorylated extracellular matrix proteins of bone and dentin. Vol. 2. Bentham Science Publishers; Oak Park (IL): 2012. p. 266-282.
3. Hunter GK, Goldberg HA. Nucleation of hydroxyapatite by bone sialoprotein. Proc Natl Acad Sci USA. 1993; 90:8562–5. [PubMed: 8397409]
4. Tye CE, Rattray KR, Warner KJ, Gordon JA, Sodek J, Hunter GK, Goldberg HA. Delineation of the hydroxyapatite-nucleating domains of bone sialoprotein. J Biol Chem. 2003; 278:7949–55. [PubMed: 12493752]
5. Baht GS, Hunter GK, Goldberg HA. Bone sialoprotein–collagen interaction promotes hydroxyapatite nucleation. Matrix Biol. 2008; 27:600–608. [PubMed: 18620053]
6. Tye CE, Hunter GK, Goldberg HA. Identification of the type I collagen-binding domain of bone sialoprotein and characterization of the mechanism of interaction. J Biol Chem. 2005; 280:13487–92. [PubMed: 15703183]
7. Gordon J, Tye C, Sampaio A, Underhill M, Hunter GK, Goldberg HA. Bone sialoprotein expression enhances osteoblast differentiation and matrix mineralization in vitro. Bone. 2007; 41:462–73. [PubMed: 17572166]
8. Bouleftour W, Juignet L, Guenaelle B, Granito RN, Vanden-Bossche A, Laroche N, Aubin JE, Lafage-Proust MH, Vico L, Malaval L. The role of the SIBLING, Bone Sialoprotein in skeletal biology - Contribution of mouse experimental genetics. Matrix Biol. 2016 [Epub ahead of print].
9. Malaval L, Wade-Guéye N, Boudiffa M, Fei J, Zirngibl R, Chen F, Laroche N, Roux JP, Burt-Pichat B, Duboeuf F, Boivin G, Jurdic P, Lafage-Proust MH, Amédée J, Vico L, Rossant J, Aubin J. Bone sialoprotein plays a functional role in bone formation and osteoclastogenesis. J Exp Med. 2008; 205:1145–53. [PubMed: 18458111]
10. Soenjaya Y, Foster BL Jr, Nociti FH, Ao M, Holdsworth DW, Hunter GK, Somerman MJ, Goldberg HA. Mechanical Forces Exacerbate Periodontal Defects in BSP-null mice. J Dent Res. 2015; 94:1276–1285. [PubMed: 26130257]
11. Monfoulet L, Malaval L, Aubin JE, Rittling SR, Gadeau AP, Fricain JC, Chassande O. Bone sialoprotein, but not osteopontin, deficiency impairs the mineralization of regenerating bone during cortical defect healing. Bone. 2010; 46:447–52. [PubMed: 19761880]

12. Wade-Gueye N, Boudiffa M, Vanden-Bossche A, Laroche N, Aubin J, Vico L, Lafage-Proust MH, Malaval L. Absence of bone sialoprotein (BSP) impairs primary bone formation and resorption: The marrow ablation model under PTH challenge. Bone. 2012; 50:1064–73. [PubMed: 22586700]
13. Foster BL, Soenjaya Y, Nociti FH, Holm E, Zerfas PM, Wimer HF, Holdsworth DW, Aubin JE, Hunter GK, Goldberg HA, Somerman MJ. Deficiency in Acellular Cementum and Periodontal Attachment in Bsp Null Mice. J Dent Res. 2013; 92:166–72. [PubMed: 23183644]
14. Foster BL, Ao M, Willoughby C, Soenjaya Y, Holm E, Lukashova L, Tran AB, Wimer HF, Zerfas PM Jr, Nociti FH, Kantovitz KR, Quan BD, Sone ED, Goldberg HA, Somerman MJ. Mineralization defects in cementum and craniofacial bone from loss of bone sialoprotein. Bone. 2015; 78:150–64. [PubMed: 25963390]
15. Benjamin M, McGonagle D. The anatomical basis for disease localisation in seronegative spondyloarthropathy at entheses and related sites. J Anat. 2001; 199:503–26. [PubMed: 11760883]
16. Fukuta S, Oyama M, Kavalkovich K, Fu FH, Niyibizi C. Identification of types II, IX and X collagens at the insertion site of the bovine achilles tendon. Matrix Biol. 1998; 17:65–73. [PubMed: 9628253]
17. Connizzo BK, Yannascoli SM, Soslowsky LJ. Structure-function relationships of postnatal tendon development: a parallel to healing. Matrix Biol. 2013; 32:106–116. [PubMed: 23357642]
18. Galatz LM, Ball CM, Teefey CM, Middleton WD. The outcome and repair integrity of completely arthroscopically repaired large and massive rotator cuff tears. The J Bone Joint Surg Am. 2004; 86:219–24. [PubMed: 14960664]
19. Genin GM, Kent A, Birman V, Wopenka B, Pasteris JD, Marquez PJ, Thomopoulos S. Functional grading of mineral and collagen in the attachment of tendon to bone. Biophys J. 2009; 97:976–85. [PubMed: 19686644]
20. Schwartz AG, Pasteris JD, Genin GM, Daulton TL, Thomopoulos S. Mineral distributions at the developing tendon enthesis. PloS One. 2012; 7:e48630. [PubMed: 23152788]
21. Hunter GK, Kyle CL, Goldberg HA. Modulation of crystal formation by bone phosphoproteins: structural specificity of the osteopontin-mediated inhibition of hydroxyapatite formation. Biochem J. 1994; 300:723–8. [PubMed: 8010953]
22. Gao J, Messner K, Ralphs JR, Benjamin M. An immunohistochemical study of enthesis development in the medial collateral ligament of the rat knee joint. Anat Embryol. 1996; 194:399–406. [PubMed: 8896704]
23. Waggett AD, Ralphs JR, Kwan AP, Woodnutt D, Benjamin M. Characterization of collagens and proteoglycans at the insertion of the human Achilles tendon. Matrix Biol. 1998; 16:457–70. [PubMed: 9550263]
24. Liu Y, Birman V, Chen C, Thomopoulos S, Genin G. Mechanisms of Bimaterial Attachment at the Interface of Tendon to Bone. J Eng Mater Technol. 2011; 133:011006. [PubMed: 21743758]
25. Liu CF, Aschbacher-Smith L, Barthelery N, Dyment N, Butler D, Wylie C. Spatial and Temporal Expression of Molecular Markers and Cell Signals During Normal Development of the Mouse Patellar Tendon. Tissue Engineering Part A. 2012; 18:598–608. [PubMed: 21939397]
26. Thomopoulos S, Williams GR. Tendon to bone healing: differences in biomechanical, structural, and compositional properties due to a range of activity levels. J Biochem Eng. 2003; 125:106–13.
27. Thomopoulos S, Marquez J, Weinberger B, Birman V, Genin G. Collagen fiber orientation at the tendon to bone insertion and its influence on stress concentrations. J Biomech. 2005; 39:1842–51. [PubMed: 16024026]
28. Liu CF, Breidenbach A, Aschbacher-Smith L, Butler D, Wylie CA. Role for Hedgehog Signaling in the Differentiation of the Insertion Site of the Patellar Tendon in the Mouse. PLoS ONE. 2013; 8:e65411. [PubMed: 23762363]
29. Dyment NA, Breidenbach AP, Schwartz AG, Russell RP, Aschbacher-Smith L, Liu H, Hagiwara Y, Jiang R, Thomopoulos S, Butler DL, Rowe DW. Gdf5 progenitors give rise to fibrocartilage cells that mineralize via hedgehog signaling to form the zonal enthesis. Dev Biol. 2015; 405:96–107. [PubMed: 26141957]
30. Breidenbach AP, Aschbacher-Smith L, Lu Y, Dyment NA, Liu CF, Liu H, Wylie C, Rao M, Shearn JT, Rowe DW, Kadler KE, Jiang R, Butler DL. Ablating hedgehog signaling in tenocytes during

development impairs biomechanics and matrix organization of the adult murine patellar tendon enthesis. J Orthop Res. 2015; 33:1142–1151. [PubMed: 25807894]

31. Schwartz AG, Long F, Thomopoulos S. Enthesis fibrocartilage cells originate from a population of hedgehog-responsive cells modulated by the loading environment. Development. 2015; 142:196–206. [PubMed: 25516975]
32. Polisson RP, Martinez S, Khoury M, Harrell RM, Lyles KW, Friedman N, Harrelson JM, Reisner E, Drezner MK. Calcification of entheses associated with X-linked hypophosphatemic osteomalacia. N Engl J Med. 1985; 313:1–6. [PubMed: 4000222]
33. Liang G, Katz L, Insogna K, Carpenter T, Macica C. Survey of the Enthesopathy of X-Linked Hypophosphatemia and Its Characterization in Hyp Mice. Calcif Tissue Int. 2009; 85:235–46. [PubMed: 19609735]
34. Lorenz-Depiereux B, Bastepe M, Benet-Pagès A, Amyere M, Wagenstaller J, Müller-Barth U, Badenhoop K, Kaiser SM, Rittmaster RS, Shlossberg AH, Olivares JL, Loris C, Ramos FJ, Glorieux F, Vikkula M, Jüppner H, Strom TM. 2006 DMP1 mutations in autosomal recessive hypophosphatemia implicate a bone matrix protein in the regulation of phosphate homeostasis. Nat Genet. 2006; 38:1248–50. [PubMed: 17033625]
35. Benjamin M, Ralphs JR. Fibrocartilage in tendons and ligaments--an adaptation to compressive load. J Anat. 1998; 193:481–94. [PubMed: 10029181]
36. Gao J, Messner K. Quantitative comparison of soft tissue-bone interface at chondral ligament insertions in the rabbit knee joint. J Anat. 1996; 188:367–73. [PubMed: 8621336]
37. Thomopoulos S, Kim HM, Rothermich SY, Biederstadt C, Das R, Galatz LM. Decreased muscle loading delays maturation of the tendon enthesis during postnatal development. J Orthop Res. 2007; 25:1154–63. [PubMed: 17506506]
38. Wang J, Zhou HY, Salih E, Xu L, Wunderlich L, Gu X, Hofstaetter J, Torres M, Glimcher M. Site-Specific In Vivo Calcification and Osteogenesis Stimulated by Bone Sialoprotein. Calcif Tissue Int. 2006; 79:179–89. [PubMed: 16969594]
39. Malaval L, Monfoulet L, Fabre T, Pothuaud L, Bareille R, Miraux S, Thiaudiere E, Raffard G, Franconi JM, Lafage-Proust MH, Aubin JE, Vico L, Amédée J. Absence of bone sialoprotein (BSP) impairs cortical defect repair in mouse long bone. Bone. 2009; 45:853–61. [PubMed: 19524706]
40. Zelzer E, Blitz E, Killian M, Thomopoulos S. 2014 Tendon-to-bone attachment: From development to maturity. Birth Defects Res C Embryo Today. 2014; 102:101–12. [PubMed: 24677726]
41. Bouleftour W, Boudiffa M, Wade-Gueye N, Bouët G, Cardelli M, Laroche N, Vanden-Bossche A, Thomas M, Bonnelye E, Aubin JE, Vico L, Lafage-Proust MH, Malaval L. Skeletal Development of Mice Lacking Bone Sialoprotein (BSP)-Impairment of Long Bone Growth and Progressive Establishment of High Trabecular Bone Mass. PloS One. 2014; 9:e95144. [PubMed: 24816232]
42. Holm E, Aubin JE, Hunter GK, Beier F, Goldberg HA. Loss of bone sialoprotein leads to impaired endochondral bone development and mineralization. Bone. 2015; 71:145–54. [PubMed: 25464126]
43. Holm E, Gleberzon JS, Liao Y, Sørensen ES, Beier F, Hunter GK, Goldberg HA. Osteopontin mediates mineralization and not osteogenic cell development in vitro. Biochem J. 2014; 464:355–364. [PubMed: 25310312]
44. Wang G, Woods A, Agoston H, Ulici V, Glogauer M, Beier F. Genetic ablation of Rac1 in cartilage results in chondrodysplasia. Dev Biol. 2007; 306:612–623. [PubMed: 17467682]
45. Tripp EJ, MacKay EH. Silver staining of bone prior to decalcification for quantitative determination of osteoid in sections. Stain Technol. 1972; 47:129–36. [PubMed: 4111887]
46. Dunkman AA, Buckley MR, Meinaltowski MJ, Adams SM, Thomas SJ, Satchell L, Kumar A, Pathmanathan L, Beason DP, Iozzo RV, Birk DE, Soslowsky LJ. Decorin expression is important for age-related changes in tendon structure and mechanical properties. Matrix Biol. 2013; 32:3–13. [PubMed: 23178232]

HIGHLIGHTS

- We identified bone sialoprotein and osteopontin in the mineralized murine fibrocartilaginous entheses
- Histological analysis of *Bsp*$^{-/-}$ mouse revealed that the quadriceps tendon enthesis in these mice are 28% longer than wild type mice at age 15 weeks
- Mechanical testing of the *Bsp*$^{-/-}$ patellar tendon revealed a thicker yet mechanically inferior tendon as compared to wild type.
- Mineral content of the *Bsp*$^{-/-}$ enthesis, as measured my micro-CT and Raman spectroscopy, is similar to that of wild type mice.

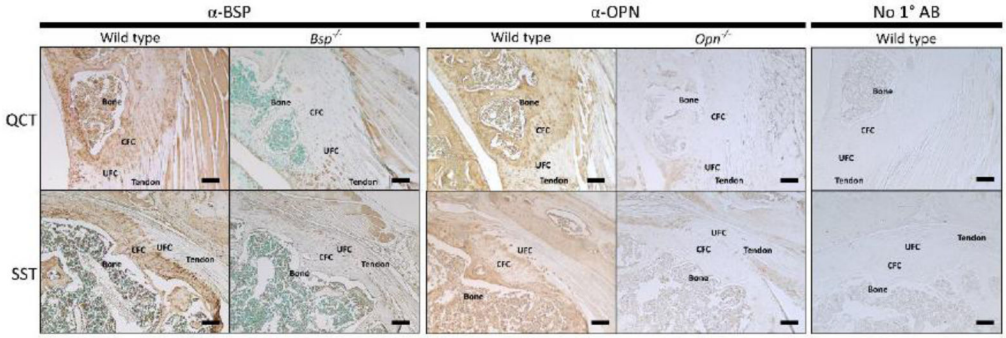

Figure 1. SIBLING proteins are present in the calcified fibrocartilage of the SST and QCT entheses

Immunohistochemistry was performed to detect the presence of BSP and OPN protein (brown staining) in the quadriceps tendon enthesis (QCT) and supraspinatus tendon enthesis (SST). BSP and OPN were detected in the bone and calcified fibrocartilage of these entheses and are not present beyond a sharp boundary representing the tidemark between the CFC and UFC. Negative controls for BSP and OPN immunostaining were performed on Bsp−/− and Opn−/− mice. No staining in the CFC of the knockout mice was detected. Animals are 15 week old male wild type 129/CD1 mice. CFC: calcified fibrocartilage, UFC: uncalcified fibrocartilage, bar = 100 μm

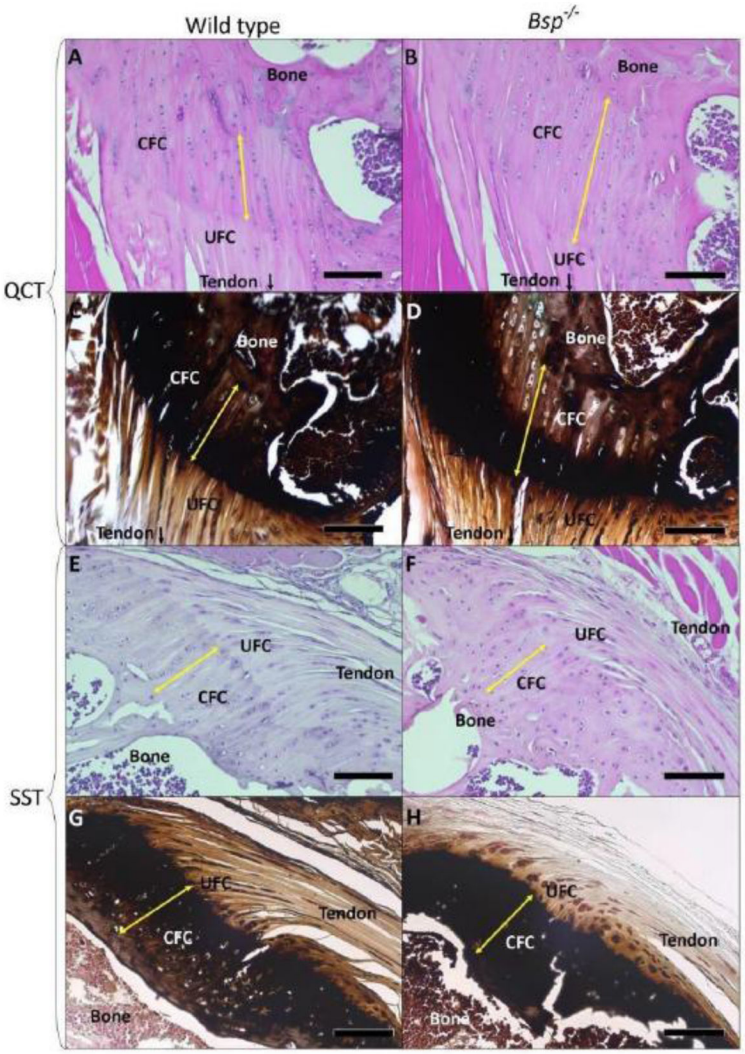

Figure 2. Morphology of the calcified fibrocartilage is altered in *Bsp*$^{-/-}$ mice

(A,B,E,F) Staining with hematoxylin and eosin was used to assess gross morphology. An extenson of the calcifed fibrocartilage was observed, as measured from tidemark to bone (yellow arrow) in the QCT enthesis (n=5). **(C,D,G,H)** Von Kossa staining of the QCT and SST entheses indicate approximately equivalent mineral content in the CFC of the wild type and *Bsp*$^{-/-}$ enthesis. CFC: calcified fibrocartilage, UFC: uncalcified fibrocartilage, bar = 100 μm

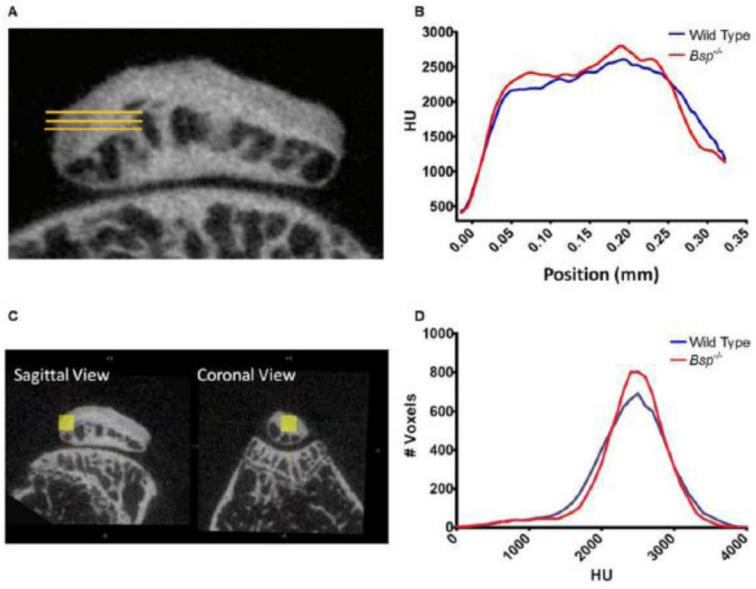

Figure 3. Micro-CT analyses indicates similar levels of mineralization in wild type and *Bsp*$^{-/-}$ QCT entheses

(A) Three parallel lines (yellow) were drawn along the known orientation of the insertion into bone to analyze changes in mineral density across the CFC. Lines span from points before the tidemark across the QCT enthesis and patellar bone into the marrow space. Positon 0.00 indicates where radiodensity crossed a threshold of 800 HU, which was estimated to be the tidemark. **(B)** Radiodensity, which is an estimate of mineral content, across the length of the QCT enthesis was similar between wild type and *Bsp*$^{-/-}$ mice. Radiodensity near the tidemark trended towards an increase in the region adjacent to the tidemark in *Bsp*$^{-/-}$ mice. **(C)** Micro-CT analysis was also performed to determine the overall radiodensity within a 20 × 20 × 20 voxel region of the CFC. However, **(D)** the results showed no apparent changes in the overall mineral density of the *Bsp*$^{-/-}$ CFC zone compared to wild type. HU: Hounsfield units.

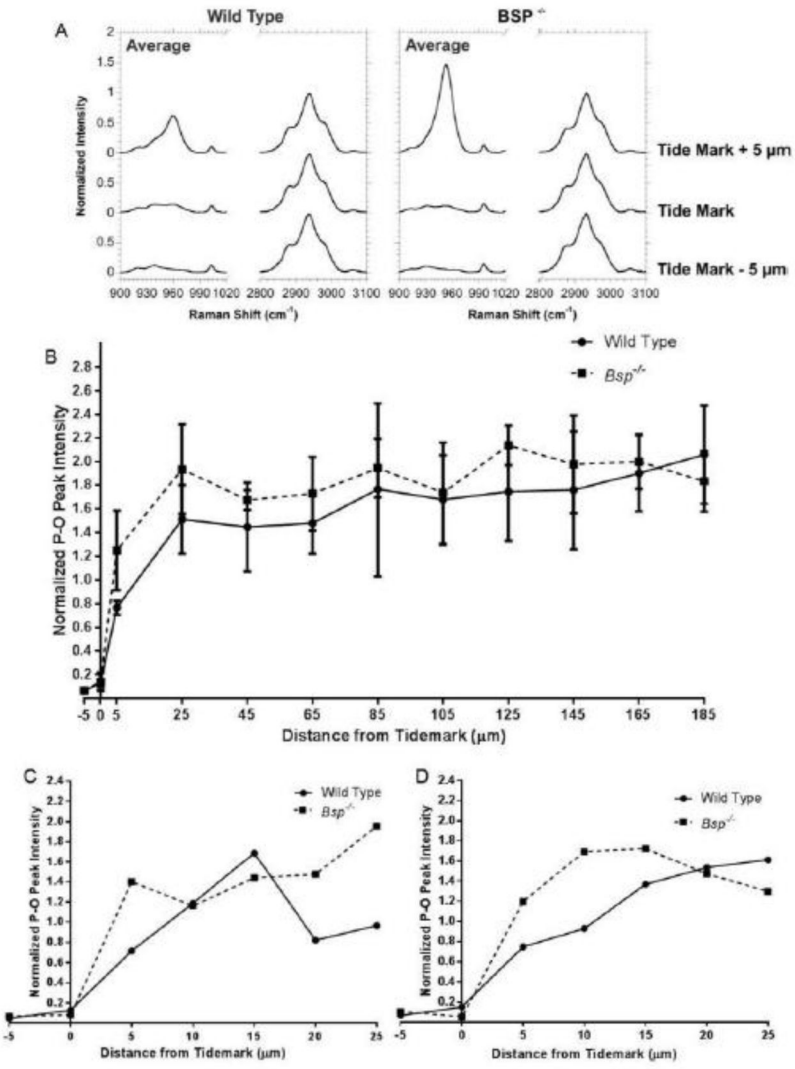

Figure 4. Raman spectroscopy shows that the mineral content in the QCT enthesis is comparable between wild type and *Bsp*$^{-/-}$ mice

(A) 960 cm^{-1} hydroxyapatite peak intensities and 2940 cm^{-1} collagen peak intensities were analyzed at the tidemark and 5 µm to either side. 960 cm^{-1} peaks are normalized to the 2940 cm^{-1} peak at each position measured. (**B)** Overall mineral content across the length of the QCT enthesis is similar between *Bsp*$^{-/-}$ and wild type mice. **(C,D)** Differences in mineral gradients are more apparent in comparisons of single lines from individual wild type and *Bsp*$^{-/-}$ littermate pairs, however overall there are no significant differences due to the high variability in mineral to collagen ratios.

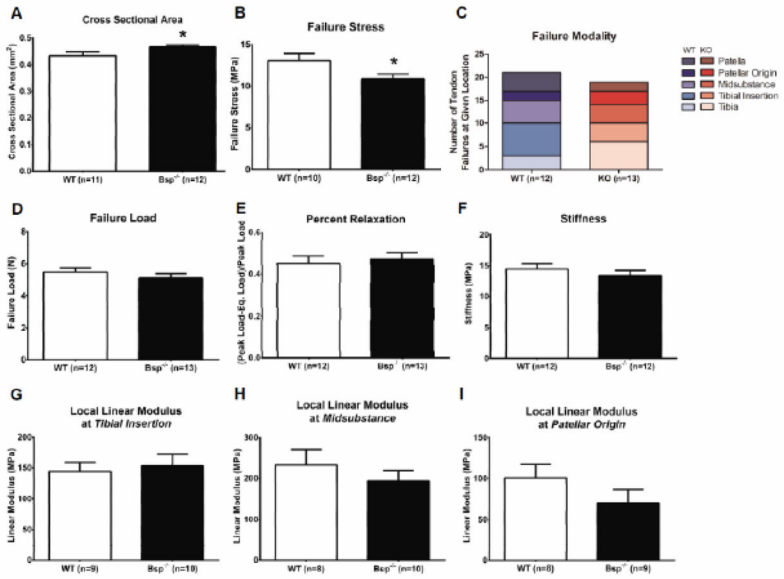

Figure 5. Bsp$^{-/-}$ mice exhibit alterations in patellar tendon mechanical properties

Various mechanical properties of the patellar tendon of 15 week-old wild type and Bsp$^{-/-}$ mice were measured. Bsp$^{-/-}$ mice patellar tendons have a larger cross-sectional area compared to wild type **(A)**. During tensile mechanical tests, the Bsp$^{-/-}$ mice patellar tendons failed at similar loads **(D)** compared to wild type, despite having a larger cross-sectional area, resulting in lower failure stress **(B)**. The failure sites varied across the tendon **(C).** Percent relaxation and stiffness of the tendons were not significantly different between genotypes **(E,F)**, nor were there any significant differences between genotypes in the linear moduli of the tendons at any site measured **(G–I)**. Values shown represent means ± SEM; *p < 0.05.

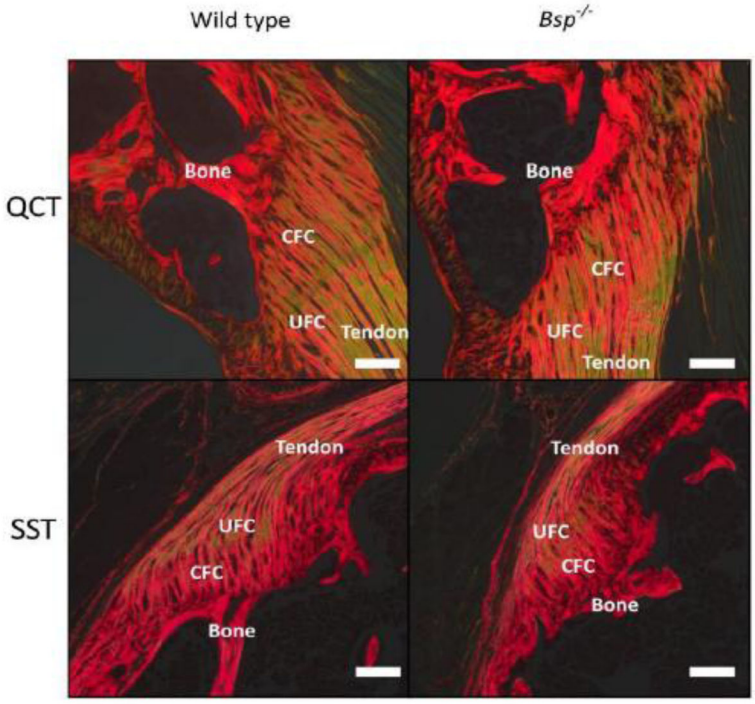

Figure 6. Collagen organization in the enthesis is not affected by loss of BSP

(A) SST and QCT entheses of wild type and *Bsp*$^{-/-}$ animals were stained using picrosirius red and viewed under circularly polarized light (n=7). Red-orange hues represent densely packed collagen fibers while greenish hues represent more loosely packed collagen fibers. CFC: calcified fibrocartilage, UFC: uncalcified fibrocartilage, bar = 100 μm

Table 1

CFC lengths of 15 week and 14 month old wild type and *Bsp*$^{-/-}$ QCT entheses

CFC length was measured by drawing three lines from tidemark to bone in the orientation of the insertion per individual mouse by two blinded observers and averaged (see Supplemental Fig 1). Average CFC lengths from wild type and *Bsp*$^{-/-}$ mice were compared against each other using a two-tailed, unpaired, parametric t-test. Statistical analysis indicated significant differences ($p<0.05$) between genotypes within the 15 week old group.

CFC Length (μm)	Wild type	*Bsp*$^{-/-}$
15 weeks (n=5)	178.8±15.5 μm	229.1±17.5 μm
14 months (n=3)	182.9±23.7 μm	259.3±17.5 μm